

Dimensional Expressivity Analysis, best-approximation errors, and automated design of parametric quantum circuits

Lena Funcke,^{a,b} Tobias Hartung,^{c,d,*} Karl Jansen,^e Stefan Kühn,^d
Manuel Schneider^{e,f} and Paolo Stornati^{e,g}

^aCenter for Theoretical Physics, Co-Design Center for Quantum Advantage, and NSF AI Institute for Artificial Intelligence and Fundamental Interactions, Massachusetts Institute of Technology, 77 Massachusetts Avenue, Cambridge, MA 02139, USA

^bPerimeter Institute for Theoretical Physics, 31 Caroline Street North, Waterloo, ON N2L 2Y5, Canada

^cDepartment of Mathematical Sciences, University of Bath, 4 West, Claverton Down, Bath, BA2 7AY, UK

^dComputation-based Science and Technology Research Center, The Cyprus Institute, 20 Kavafi Street, 2121 Nicosia, Cyprus

^eDeutsches Elektronen-Synchrotron DESY, Platanenallee 6, 15738 Zeuthen

^fInstitut für Physik, Humboldt-Universität zu Berlin, Newtonstraße 15, 12489 Berlin, Germany

^gICFO, The Barcelona Institute of Science and Technology, Av. Carl Friedrich Gauss 3, 08860 Castelldefels (Barcelona), Spain

E-mail: lfuncke@mit.edu, tobias.hartung@desy.de, s.kuehn@cyi.ac.cy,

karl.jansen@desy.de, manuel.schneider@desy.de, paolo.stornati@desy.de

The design of parametric quantum circuits (PQCs) for efficient use in variational quantum simulations (VQS) is subject to two competing factors. On one hand, the set of states that can be generated by the PQC has to be large enough to contain the solution state. Otherwise, one may at best find the best approximation of the solution restricted to the states generated by the chosen PQC. On the other hand, the PQC should contain as few parametric quantum gates as possible to minimize noise from the quantum device. Thus, when designing a PQC one needs to ensure that there are no redundant parameters. The dimensional expressivity analysis discussed in these proceedings is a means of addressing these counteracting effects. Its main objective is to identify independent and redundant parameters in the PQC. Using this information, superfluous parameters can be removed and the dimension of the space of states that are generated by the PQC can be computed. Knowing the dimension of the physical state space then allows us to deduce whether or not the PQC can reach all physical states. Furthermore, the dimensional expressivity analysis can be implemented efficiently using a hybrid quantum-classical algorithm. This implementation has relatively small overhead costs both for the classical and quantum part of the algorithm and could therefore be used in the future for on-the-fly circuit construction. This would allow for optimized circuits to be used in every loop of a VQS rather than the same PQC for the entire VQS. These proceedings review and extend work in [1, 2].

Preprint number: MIT-CTP/5349

*The 38th International Symposium on Lattice Field Theory, LATTICE2021 26th-30th July, 2021
Zoom/Gather@Massachusetts Institute of Technology*

*Speaker

1. Introduction

The fast development of noisy intermediate-scale quantum (NISQ) computers [3] builds the foundation for a large class of computational problems that cannot be solved efficiently with classical computers to be addressed with quantum devices. Such applications of quantum computing include machine learning [4], finance [5], various optimization problems [6, 7], as well as physics. A great advantage of quantum computation in physics is that it can circumvent the sign problem which prevents Monte Carlo simulations of many strongly correlated quantum-many body problems [8]. Although current quantum hardware is of limited size and suffers from a considerable level of noise, NISQ devices have already successfully demonstrated their ability to outperform classical computers [9, 10] and techniques for mitigating the effects of noise are rapidly developing [11–15].

An important class of algorithms designed for NISQ devices are variational quantum simulations (VQs) [16, 17]. These are hybrid quantum-classical algorithms for solving optimization problems and make use of parametric quantum circuits (PQCs), i.e., quantum circuits composed of parameter dependent gates. VQs generally consist of a classical feedback loop optimizer that aims to minimize a given cost function which can be evaluated efficiently using the quantum device as a co-processor. In many cases, the cost function is related to the energy of the quantum state prepared on the quantum device by the PQC at a given set of parameters. As such, VQs are naturally attuned to applications in quantum many-body systems in quantum chemistry [12, 16, 18, 19], as well as in quantum mechanics and quantum field theory [20–24].

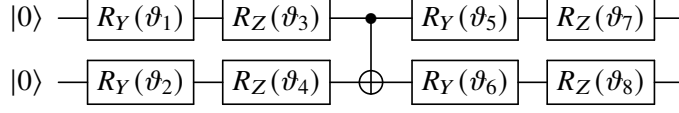
Since VQs intrinsically depend on the design of PQCs, finding a good or optimal PQC is paramount. This naturally leads to counteracting effects that need to be balanced. For example, in order to be able to find the solution, a PQC needs to have many parameters. If there are too few parameters, there will be physically relevant states which cannot be expressed with the given PQC. However, many parameters means many gates and thus large noise. Being able to express all physically relevant states is therefore one measure for being a “good” PQC. Taking this point of view, an “optimal” PQC would not only be *maximally expressive* (the circuit can generate all relevant states) but also *minimal* (there are no redundant parameters, i.e., removing any parameter would reduce the set of states the PQC can generate). Analyzing PQCs from this point of view is the main objective of the dimensional expressivity analysis (DEA) [1, 2].

In these proceedings, we will review the theoretical background of the DEA in [section 2](#) and the hardware implementation in [section 3](#). In [section 4](#) we will review physical state spaces, which allows us to find a termination condition for PQC construction schemes that can have arbitrarily many parameters, and which allows us to automate custom circuit designs. In particular, the here presented automated circuit design explicitly extend the results of [1]. Finally, we will review best-approximation error estimates in [section 5](#) and provide some concluding remarks in [section 6](#).

2. Theoretical Background

In this section, we will discuss the theoretical background of the dimensional expressivity analysis. At the most fundamental level, the DEA aims to identify redundant parameters in a given PQC. To this end, we consider a *parametric quantum circuit* to be a map C from some parameter space \mathcal{P} into the state space \mathcal{S} . The state space \mathcal{S} may be the entire state space of the quantum

device or just contain the physically relevant states. As such, the PQC includes the quantum device initialization, and for each set of parameters $\vartheta \in \mathcal{P}$, $C(\vartheta)$ is a state of the quantum device. For example,



is a PQC on a two-qubit device with initial state $|0\rangle \otimes |0\rangle$. The parametric gates in this circuit are rotation gates $R_G(\vartheta) = \exp(-\frac{i}{2}\vartheta G)$, where G is a Pauli matrix Y or Z depending on the gate. For the purpose of these proceedings, we will restrict our considerations to such rotation gates R_G with $G = X, Y, Z$. We refer to [1, 2] for treatments of more general gates, such as $G = \text{CNOT}(c, t)$ or $G = \sum_{q=0}^{Q-1} X_q X_{q+1}$ where X_q is a Pauli X gate acting on qubit q . In complete generality, any parametric dependence on the unitary operation performed on the quantum device can be considered.

2.1 Identification of redundant parameters

A parameter ϑ_k is considered to be *redundant* if a small change of ϑ_k keeping all other ϑ_j fixed produces a state that can also be obtained by keeping ϑ_k fixed and adjusting all other ϑ_j accordingly. Geometrically speaking, this means that the partial derivative $\partial_k C(\vartheta)$ of C with respect to ϑ_k is a linear combination of the remaining partial derivatives $\partial_j C(\vartheta)$. This can be checked inductively by considering the real partial Jacobians J_k of C ,

$$J_k(\vartheta) = \begin{pmatrix} \Re \partial_1 C(\vartheta) & \cdots & \Re \partial_k C(\vartheta) \\ \Im \partial_1 C(\vartheta) & \cdots & \Im \partial_k C(\vartheta) \end{pmatrix}. \quad (1)$$

As long as ϑ_1 is non-trivial, J_1 will always have rank 1. Adding the column for $\partial_2 C$, we can check whether J_2 has rank 2. If that is the case, then we move on to the next parameter. If adding a column for $\partial_k C$ does not increase the rank of J_k , then ϑ_k is redundant and can be set constant. This effectively removes the parameter and thus the corresponding column in J_k . Eventually, either all parameters have been checked and classified as independent/redundant or the number of independent parameters found equals the dimension of \mathcal{S} . In the latter case, we can stop the analysis as all further parameters must necessarily be dependent.

It should be noted that the choice of the *real* partial Jacobian is necessitated by the fact that our parameter space \mathcal{P} is commonly a real manifold. Thus, the linear dependence check has to be performed with respect to linear combinations in \mathbb{R} as opposed to \mathbb{C} .

To check the rank of J_k efficiently, we usually consider the matrix $S_k = J_k^* J_k$ instead. Since, by induction, we can assume that J_{k-1} has full rank, J_k has full rank if and only if all eigenvalues of S_k are strictly positive. Thus, computing the smallest eigenvalue of S_k (or otherwise checking S_k for invertibility) only has a computational complexity in $\mathcal{O}(k^3)$ and does not require working with the J_k directly which are of dimension $2^{Q+1} \times k$ where Q is the number of qubits. Alternatively, if the number of parameters N for a given PQC is fixed (i.e., the PQC is not given by a construction that can use arbitrarily many parameters), computing the reduced row echelon form of S_N can also identify all independent parameters.

2.2 Two Bloch sphere examples

To illustrate the analysis, let us consider two quantum circuits on a single qubit. The first circuit will have two independent parameters. The second circuit will have one dependent parameter.

2.2.1 A minimal circuit

The first circuit we want to consider is $C(\vartheta) = R_Z(\vartheta_2)R_X(\vartheta_1)|0\rangle$. Using $|0\rangle$ and $|1\rangle$ as a basis of the single-qubit Hilbert space, we can write

$$C(\vartheta) = R_Z(\vartheta_2)R_X(\vartheta_1)|0\rangle = \begin{pmatrix} \cos \frac{\vartheta_1}{2} \cos \frac{\vartheta_2}{2} - i \cos \frac{\vartheta_1}{2} \sin \frac{\vartheta_2}{2} \\ -i \sin \frac{\vartheta_1}{2} \cos \frac{\vartheta_2}{2} + \sin \frac{\vartheta_1}{2} \sin \frac{\vartheta_2}{2} \end{pmatrix} \begin{pmatrix} |0\rangle \\ |1\rangle \end{pmatrix}, \quad (2)$$

which yields

$$J_1 = \frac{1}{2} \begin{pmatrix} -\sin \frac{\vartheta_1}{2} \cos \frac{\vartheta_2}{2} \\ \cos \frac{\vartheta_1}{2} \sin \frac{\vartheta_2}{2} \\ \sin \frac{\vartheta_1}{2} \sin \frac{\vartheta_2}{2} \\ -\cos \frac{\vartheta_1}{2} \cos \frac{\vartheta_2}{2} \end{pmatrix} \quad \text{and} \quad J_2 = \frac{1}{2} \begin{pmatrix} -\sin \frac{\vartheta_1}{2} \cos \frac{\vartheta_2}{2} & -\cos \frac{\vartheta_1}{2} \sin \frac{\vartheta_2}{2} \\ \cos \frac{\vartheta_1}{2} \sin \frac{\vartheta_2}{2} & \sin \frac{\vartheta_1}{2} \cos \frac{\vartheta_2}{2} \\ \sin \frac{\vartheta_1}{2} \sin \frac{\vartheta_2}{2} & -\cos \frac{\vartheta_1}{2} \cos \frac{\vartheta_2}{2} \\ -\cos \frac{\vartheta_1}{2} \cos \frac{\vartheta_2}{2} & \sin \frac{\vartheta_1}{2} \sin \frac{\vartheta_2}{2} \end{pmatrix} \quad (3)$$

and hence

$$S_1 = J_1^* J_1 = \frac{1}{4} \quad \text{and} \quad S_2 = J_2^* J_2 = \begin{pmatrix} \frac{1}{4} & 0 \\ 0 & \frac{1}{4} \end{pmatrix}. \quad (4)$$

Both S_1 and S_2 are invertible. This implies that both parameters are independent. Since neither parameter can be removed without reducing the expressivity of the circuit, this circuit is minimal.

2.2.2 A reducible circuit

If instead we consider the circuit $C(\vartheta) = R_X(\vartheta_2)R_X(\vartheta_1)|0\rangle$, then the same analysis yields

$$S_1 = J_1^* J_1 = \frac{1}{4} \quad \text{and} \quad S_2 = J_2^* J_2 = \frac{1}{4} \begin{pmatrix} 1 & 1 \\ 1 & 1 \end{pmatrix}. \quad (5)$$

Here, S_1 is invertible, i.e., the first X -rotation gate is independent. However, S_2 is not invertible and we have correctly identified that the second X -rotation has no contribution to the circuit that cannot already be achieved with the first X -rotation. Thus, ϑ_2 is redundant and can be removed, that is, it can be set to a constant value. Depending on the circumstances, this constant value could be chosen to be 0, thus removing the gate from the circuit, or it may be advantageous to keep ϑ_2 at a non-trivial value. The latter would be more common in experimental setups where the dependent parameter may be a pulse duration and thus only certain values are experimentally viable, or this choice may be employed in on-the-fly circuit construction with seamless switching [1].

2.3 Removal of unwanted symmetries

An important extension to the basic parameter identification is the ability to remove unwanted symmetries from a PQC. This may occur if a PQC should be constructed to be invariant under some symmetry that has no impact on the cost function, e.g., gauge invariance or more simply a global

phase symmetry. As the symmetry has no impact on the cost function, removing any parameters that only contribute this symmetry would further improve the efficiency of many classical feedback loop optimizers used in the VQS. Moreover, this would likely reduce the amount of device noise because fewer gates need to be employed in the PQC.

To remove the unwanted symmetry, we need to formally extend the PQC $C(\vartheta)$ to a larger circuit $\tilde{C}(\varphi, \vartheta)$ in such a way that (a) keeping ϑ fixed and varying φ only changes $\tilde{C}(\varphi, \vartheta)$ by the action of the unwanted symmetry and (b) there exists a φ_0 such that $\tilde{C}(\varphi_0, \vartheta) = C(\vartheta)$.

For example, let us consider the circuit $C(\vartheta) = R_Y(\vartheta_3)R_Z(\vartheta_2)R_X(\vartheta_1)|0\rangle$. This circuit is minimal and can generate every single-qubit state. Thus, for every $\vartheta \in (\mathbb{R}/2\pi\mathbb{Z})^3$ and $\alpha \in U(1)$, there exists a ϑ' such that $C(\vartheta') = \alpha C(\vartheta)$. In this sense, C has a global phase symmetry. To remove this symmetry, we extend C to the circuit $\tilde{C}(\varphi, \vartheta) = R_Y(\vartheta_3)R_Z(\vartheta_2)R_X(\vartheta_1)R_Z(\varphi)|0\rangle$. Thus, keeping ϑ fixed and changing $\varphi \rightarrow \varphi'$ only produces a phase change $e^{-i\frac{\varphi' - \varphi}{2}}$ (property (a)) and $\tilde{C}(0, \vartheta) = C(\vartheta)$ (property (b)).

To finally remove the unwanted symmetry, we perform the DEA checking the parameters φ before ϑ . This ensures that the unwanted symmetry is generated using φ , and any parameter ϑ_k that only contributes the unwanted symmetry will now be dependent on φ and all ϑ_j with $j < k$. Setting φ to φ_0 in the reduced circuit successfully removes the unwanted symmetry from the PQC.

In the case of $\tilde{C}(\varphi, \vartheta) = R_Y(\vartheta_3)R_Z(\vartheta_2)R_X(\vartheta_1)R_Z(\varphi)|0\rangle$, DEA shows that ϑ_3 is dependent, i.e., we can reduce the circuit to $\tilde{C}_r(\varphi, \vartheta) = R_Z(\vartheta_2)R_X(\vartheta_1)R_Z(\varphi)|0\rangle$ which is still maximally expressive on a single qubit. Setting $\varphi = 0$ thus yields the reduced circuit $C_r(\vartheta) = R_Z(\vartheta_2)R_X(\vartheta_1)|0\rangle$ which can generate arbitrary single-qubit states up to a global phase.

3. Hardware Implementation

If the DEA is to be used for quantum circuits on many qubits and even in on-the-fly circuit construction/optimization, then an efficient automation of the process is paramount. In subsection 2.1 we have noted that the $k \times k$ matrices $S_k = J_k^* J_k$ need to be checked for invertibility. For PQCs with N parameters, this invertibility check can be performed for all k with $O(N^2)$ memory requirements and $O(N^4)$ CPU calls. However, a classical computation of the S_k requires $O(N 2^{Q+1})$ computational resources where Q is the number of qubits. This is prohibitively expensive in the scaling limit. Thus, the computation of S_k should make use of the quantum device.

Considering $S_k = J_k^* J_k$, we note that the (m, n) -element of S_k is given by $\Re\langle \partial_m C(\vartheta), \partial_n C(\vartheta) \rangle$. Furthermore, if each parametric gate in C is a rotation gate R_{G_m} , then $\partial_m C(\vartheta) = -\frac{i}{2} \gamma_m |\text{init}\rangle$, where $\gamma_m |\text{init}\rangle$ is the circuit $C(\vartheta)$ with an additional gate G_m inserted after $R_{G_m}(\vartheta_m)$, and $|\text{init}\rangle$ is the initial state of the quantum device. Thus, the (m, n) -element of S_k is given by $\frac{1}{4} \Re\langle \text{init} | \gamma_m^* \gamma_n | \text{init} \rangle$ and the computational objective becomes measuring $\Re\langle \text{init} | \gamma_m^* \gamma_n | \text{init} \rangle$ on the quantum device.

To measure $\Re\langle \text{init} | \gamma_m^* \gamma_n | \text{init} \rangle$ on the quantum device, we can construct the state [25]

$$|\psi_{m,n}\rangle = \frac{|0\rangle \otimes (\gamma_m |\text{init}\rangle + \gamma_n |\text{init}\rangle) + |1\rangle \otimes (\gamma_m |\text{init}\rangle - \gamma_n |\text{init}\rangle)}{2} \quad (6)$$

since measuring the ancilla of $|\psi_{m,n}\rangle$ yields

$$\text{prob}(\text{ancilla} = |0\rangle) = \frac{1 + \Re\langle \text{init} | \gamma_m^* \gamma_n | \text{init} \rangle}{2}. \quad (7)$$

This can be achieved with the circuit

$$\begin{array}{c}
 \text{init} \rangle \text{---} \gamma_n \text{---} \gamma_m \text{---} \\
 \text{ancilla: } |0\rangle \text{---} H \text{---} \bullet \text{---} X \text{---} \bullet \text{---} X \text{---} H \text{---} \text{meter}
 \end{array} \quad (8)$$

using just one ancilla qubit. In fact, since γ_m and γ_n only differ by the application of G_m after R_{G_m} in γ_m and G_n after R_{G_n} in γ_n , it suffices to apply the circuit $C(\vartheta)$ once and only use controlled G_m and controlled G_n gates at the appropriate time. For example, if we consider $\Re \langle 0 | \gamma_2^* \gamma_1 | 0 \rangle$ for $C(\vartheta) = R_Z(\vartheta_2)R_X(\vartheta_1) |0\rangle$, then the circuit (8) becomes

$$\begin{array}{c}
 |0\rangle \text{---} R_X(\vartheta_1) \text{---} X \text{---} R_Z(\vartheta_2) \text{---} Z \text{---} \\
 |0\rangle \text{---} H \text{---} \bullet \text{---} X \text{---} \bullet \text{---} X \text{---} H \text{---} \text{meter}
 \end{array} \quad (9)$$

which requires only CNOT and CZ gates and not the CR_X and CR_Z gates formally required by the circuit (8).

3.1 Experimental results

In Figure 1 we show the results of the hybrid quantum-classical DEA implementation for the single-qubit circuit $C(\vartheta) = R_Y(\vartheta_4)R_Z(\vartheta_3)R_X(\vartheta_2)R_Z(\vartheta_1) |0\rangle$ at a randomly selected value of ϑ . We already know from subsection 2.3 that the parameters ϑ_1 , ϑ_2 , and ϑ_3 are independent and ϑ_4 is redundant. Thus, we expect to see that the smallest eigenvalue of S_4 is compatible with zero and all other eigenvalues are strictly positive. Figure 1 shows the two smallest eigenvalues for S_2 , S_3 , and S_4 as computed using `ibmq_ourense` and `ibmq_vigo` as co-processors. In particular, Figure 1 demonstrates that we can reliably identify ϑ_4 as redundant and the other parameters as independent.

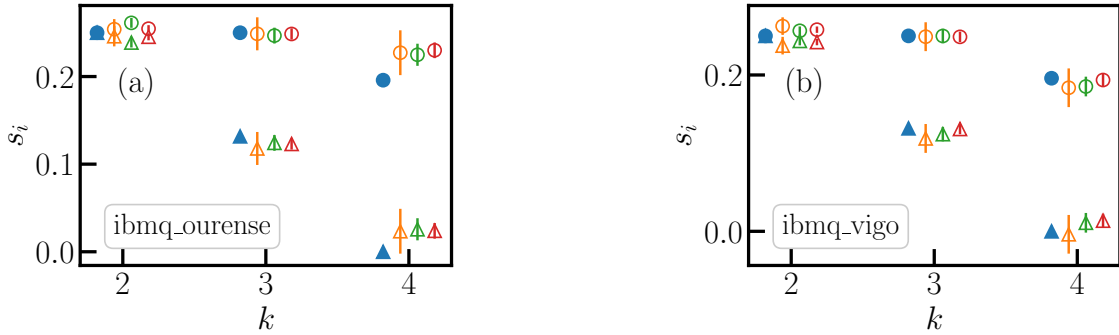


Figure 1: Single-qubit experiments on (a) `ibmq_ourense` and (b) `ibmq_vigo` quantum hardware. We show the smallest (triangles) and second smallest (dots) eigenvalues of the matrix S_k . The filled symbols are the exact solutions. The open symbols represent different statistics: orange, green and red markers stand for 1000, 4000 and 8000 shots, respectively. The error bars for the experimental data represent the uncertainty from the finite number of shots. This figure is discussed in more detail in [26].

The error bars in Figure 1 have been obtained using experimental reconstruction. Since the eigenvalues are computed from probabilities of finding the ancilla in $|0\rangle$, we do not have direct access to the error statistics of the matrices S_k . Instead, we used the observed $\text{prob}(\text{ancilla} = |0\rangle)$ and simulated 1000 experimental outcomes with this underlying probability distribution. As such, we can estimate the standard deviation of the eigenvalues. This is shown as error bars in Figure 1.

4. Physical state spaces

Since the quantum device state space grows exponentially with the number of qubits, having maximally expressive PQCs on the entire quantum device state space requires exponentially many parameters as well. This quickly leads to situations in which maximally expressive circuits are not computationally viable. However, in many physically relevant models, it is not necessary to have maximally expressive PQCs on the entire quantum device state space, since physical symmetries restrict the physically relevant state space to a dimension that grows only polynomially in the number of qubits. Thus, if we can construct a PQC that satisfies many of the physically relevant symmetries, then we only need polynomially many parameters and might be able to further reduce the number of parameters by removing any unwanted symmetries (cf., [subsection 2.3](#)).

For example, if we consider translational symmetry, then any physical state has to be invariant under the translation operator τ_Q which maps the computational basis state $|b_{Q-1} \dots b_0\rangle$ to $|b_{Q-2} \dots b_0 b_{Q-1}\rangle$, i.e., $\tau_3(|101\rangle) = |011\rangle$. In general, we may consider a symmetry operator τ on Q qubits. Then, the physical sectors are intersections of the eigenspaces of τ with the quantum device state space, i.e., the unit spheres in the eigenspaces of τ .

To analyze such physical sectors [1], we consider the action of τ on the computational basis and construct equivalence classes of states under the action of τ . Hence, $|\psi\rangle \sim_\tau |\varphi\rangle$ if $|\psi\rangle = \tau^j |\varphi\rangle$ for some j . In case of translational symmetry, $|011\rangle \sim_{\tau_3} |101\rangle$ but $|011\rangle \not\sim_{\tau_3} |001\rangle$. As such, we obtain equivalence classes $[[b]]$ and the order of an equivalence class is the number of elements in the equivalence class, i.e., $[[011]] = \{|011\rangle, |110\rangle, |101\rangle\}$ has order 3. Similarly, the eigenvalues of τ have an order. For the translational invariance case, the eigenvalues are roots of unity ω and their order is the smallest $j \geq 1$ with $\omega^j = 1$. This implies that an equivalence class $[[b]]$ can be mapped into the physical sector of an eigenvalue ω if the order of ω divides the order of $[[b]]$. Explicitly, for translational invariance, the basis vectors of this mapping can be chosen to be

$$e(\omega, [[b]]) = \frac{1}{\sqrt{\text{order}([[b]])}} \sum_{j=0}^{\text{order}([[b]])-1} \omega^j \tau_Q^j |b\rangle. \quad (10)$$

This allows us to compute the dimension of the physical sector corresponding to the eigenvalue ω with order d on Q qubits as [1]

$$\dim_{\mathbb{R}}(\text{Physical Sector of } \omega) = -1 + 2 \sum_{d|k|Q} \frac{\#(k)}{k} \quad (11)$$

where $\#(1) = 2$ and $\#(k) = 2^k - \sum_{k'|k, k' < k} \#(k')$.

[Equation 11](#) is also the number of independent parameters that a maximally expressive PQC mapping into this sector has. Hence, once this number of independent parameters is reached, all other parameters that a PQC may have must necessarily be redundant.

4.1 Automatic custom circuit construction

In this section, we will extend the results of [1] to explicitly address the question of automating the custom circuit construction described in [1]. More precisely, the equivalence class construction can be exploited for automatic custom circuit design. We will first discuss how to construct the

gates from the equivalence relations. As a second step, we will order the constructed gates based on how complicated they are to obtain an inductive automation process.

As an example, let us consider the case of the $\omega = 1$ sector of translational invariance on Q qubits. Based on Eq. (10), we can write the states in this sector of the form $e_{[|B\rangle]} = e(1, [|B\rangle]) = \{\text{order}([|B\rangle])\}^{-1/2} \sum_{|b\rangle \in [|B\rangle]} |b\rangle$. If we consider the point $|0\rangle$, then we need to construct parametric gates whose derivatives at $|0\rangle$ point into the directions $e_{[|B\rangle]}$ both with a real and an imaginary coefficient.

Starting with $|B\rangle \neq |0\rangle$, we first aim to construct a gate that generates a component in direction $e_{[|B\rangle]}$ with an imaginary coefficient. For this, we can consider the gate

$$R_{XB}(\vartheta) = \exp\left(-i\frac{\vartheta}{2} \sum_{j=0}^{\text{order}([|B\rangle])-1} X^{\tau_Q^j |B\rangle}\right), \quad (12)$$

where $X^b = X_{Q-1}^{b_{Q-1}} \otimes \dots \otimes X_0^{b_0}$. Then, $R'_{XB}(0)|0\rangle = -\frac{i}{2} (\text{order}([|B\rangle]))^{1/2} e_{[|B\rangle]}$, i.e., this gate generates a component in direction $ie_{[|B\rangle]}$ at $|0\rangle$.

As a next step, we aim to construct a gate that generates a component in direction $e_{[|B\rangle]}$ with a real coefficient. Since $B = B_{Q-1} \dots B_0 \neq 0$, at least one of the B_j is not 0, and we can choose one qubit j and replace $X_j^{B_j}$ with $Y_j^{B_j}$. For example, for $B = 101$, $B_0 \neq 0$ and $X^B = X_2 \otimes X_0$ is changed to $X_2 \otimes Y_0$. For the translational symmetry in Equation 12, $X_2 \otimes Y_0$ is shifted in the qubit index through the action of τ_Q^j , which creates operators $X_{j+2} \otimes Y_j$. Summing all these operators to replace the sum in Equation 12 results in a gate $R_{(X|Y)^B}(\vartheta)$, e.g.,

$$R_{(X|Y)^{101}}(\vartheta) = \exp\left(-i\frac{\vartheta}{2} (X_2 \otimes Y_0 + X_0 \otimes Y_1 + X_1 \otimes Y_2)\right). \quad (13)$$

By replacing exactly one X with Y , $R_{(X|Y)^B}$ generates a component in direction $e_{[|B\rangle]}$ at $|0\rangle$.

All these gates R_{XB} and $R_{(X|Y)^B}$ for $B \neq 0$ have independent parameters, as can be verified using DEA. The number of parameters is exactly one fewer than the dimension of the physical state space, and the missing gate at $|0\rangle$ should generate a component in the $i|0\rangle$ direction. This can be achieved with a translationally invariant Z -rotation gate

$$R_{Z,Q}(\vartheta) = \exp\left(-i\frac{\vartheta}{2} \sum_{q=0}^{Q-1} Z_q\right). \quad (14)$$

Considering the set of gates $R_{Z,Q}$, R_{XB} and $R_{(X|Y)^B}$, we can “order” them with respect to the number of X or Y gates acting simultaneously in each summand of the exponent in Equation 12. As such, $R_{Z,Q}$ is an order-0 gate and a gate of order k corresponds to R_{XB} or $R_{(X|Y)^B}$, where B has exactly k values $B_j = 1$. This allows for the process to be automated by inductively generating more complicated gates. Using translational invariance and the fact that we are always summing over all elements of an equivalence class $[|B\rangle]$, we can choose a “canonical” representative B of $[|B\rangle]$ by assuming $B_0 = 1$ and $B_{Q-1} = 0$. This reduces the automation procedure to a combinatorial problem with complexity that is comparable to the dimensional scaling of the physical state space dimension. In other words, if the physical state space grows polynomially in the number of qubits, then this approach generates minimal and maximally expressive custom circuits with polynomially many parameters.

5. Best-approximation error

In some cases, having maximally expressive circuits may still be computationally too costly, even with targeted custom circuits that only generate physically relevant states. Thus, it is necessary to settle for non-maximally expressive PQCs. This means that some physically relevant states cannot be reached by the PQC C and thus cannot be expressed as a state $C(\vartheta)$. In this case, we wish to compute the worst-case distance between a physically relevant $|\psi\rangle$ and the closest state $C(\vartheta)$. This worst-case distance is the (worst-case) best-approximation error α_C of the circuit C .

In order to approximate α_C , we generate a discrete sample set \mathcal{D} of N points $C(\vartheta_1), \dots, C(\vartheta_N)$. If every point $C(\vartheta)$ is ε -close to at least one point in \mathcal{D} , then we can compute the worst-case best-approximation error $\alpha_C^{\mathcal{D}}$ with respect to points in \mathcal{D} , rather than the entire image of C , and obtain $\alpha_C^{\mathcal{D}} - \varepsilon \leq \alpha_C \leq \alpha_C^{\mathcal{D}}$ [2]. Thus, if \mathcal{D} becomes dense for $N \rightarrow \infty$, we obtain $\alpha_C^{\mathcal{D}} \rightarrow \alpha_C$, and for each ε , we find a lower and upper bound on α_C . Since \mathcal{D} is a finite discrete set, we can compute $\alpha_C^{\mathcal{D}}$ using Voronoi diagrams [27, 28] in the physical state space. In particular, choosing \mathcal{D} using a scrambled Sobol' sequence in parameter space shows a convergence of $\alpha_C^{\mathcal{D}} \rightarrow \alpha_C$ that is comparable to the theoretically optimal rate of convergence [2]. However, since the Voronoi diagram computation is classical, we need an efficient mapping of the quantum states $C(\vartheta_j)$ in \mathcal{D} into classical memory. We proposed [2] to do this by constructing a basis transformation from the linear space spanned by \mathcal{D} to $\mathbb{R}^{\dim_{\mathbb{R}} \mathcal{S}+1}$, where \mathcal{S} is the relevant state space. To this end, we need to compute $\Re\langle C(\vartheta_j), C(\vartheta_k) \rangle$, which we can perform efficiently using the circuit (8). Thus, if the physically relevant state space has polynomial scaling in the number of qubits, then this hybrid quantum-classical algorithm of computing $\alpha_C^{\mathcal{D}}$ is as efficient as the Voronoi diagram computation.

Since computing Voronoi diagrams for large \mathcal{D} still requires significant computational resources, it may be useful to have a more computationally efficient lower-bound estimate of α_C . If C is known to be non-maximally expressive, then we can show $\alpha_C \gtrsim 4\pi^{\frac{\dim \mathcal{M}}{2}+1} \Gamma\left(\frac{\dim \mathcal{M}}{2}\right)^{-1} \text{vol}(\mathcal{M})^{-1}$, where \mathcal{M} is the image manifold of C [2]. Assuming C is minimal (as can be ensured using DEA), $\dim \mathcal{M}$ is the number of parameters in C and $\text{vol}(\mathcal{M}) = \int_{\mathcal{P}} \sqrt{\det g(\vartheta)} d\text{vol}_{\mathcal{P}}(\vartheta)$ can be computed using a suitable quadrature rule in the parameter space \mathcal{P} . Most importantly, g is the same matrix as S_N in subsection 2.1, i.e., we already know an efficient hybrid quantum-classical algorithm to compute this lower-bound estimate on α_C . Furthermore, we have observed that this lower-bound estimate is tight for spiral circuits on a single qubit [2].

6. Conclusion

Given a parametric quantum circuit (PQC), DEA [1, 2] allows us to identify redundant parameters in the PQC, i.e., parameters that do not increase the set of states the PQC can generate. This identification is based on an inductive procedure described in subsection 2.1, which can be automated and efficiently implemented using the hybrid quantum-classical algorithm proposed in section 3. The single-qubit experimental results of subsection 3.1 and [1] demonstrate that we can reliably classify parameters. However, we have observed in [1] that current levels of hardware noise notably affect DEA on multiple qubits. It is therefore prudent to employ low-overhead error mitigation techniques if DEA is to be used for on-the-fly circuit construction/optimization.

For efficient use of the DEA, it is beneficial to start with a PQC design that takes certain physical symmetries into account (section 4) or is at least partially optimized [2]. Then, the PQC can be further optimized by removing any unwanted symmetries (subsection 2.3). A partially optimized starting point could be a minimal and maximally expressive circuit on the entire quantum device state space as proposed in [2]. Alternatively, physical symmetries can be used for efficient termination conditions for parameter checks and automatic custom circuit construction (section 4).

Despite our optimization procedure, there may be cases in which it is too computationally costly to have a maximally expressive PQC, e.g., due to hardware limitations. In these cases, a suitable candidate PQC can be chosen as a starting point and DEA can still provide minimal PQCs with the same expressivity the initial candidate PQC has. Furthermore, the DEA can be extended to include a priori estimates of the best-approximation error through the ideas outlined in section 5. In particular, lower bounds on the best-approximation error can be achieved with a computational overhead comparable to the DEA overhead for the given circuit itself. This can be extended to obtain asymptotically tight lower and upper bounds using a Voronoi diagram-based approach.

Of course, for current NISQ devices, the application range of DEA is still limited. To make DEA an integral part of PQC design, construction, and optimization, there are two main obstacles to overcome. On the one hand, hardware noise is still a limiting factor as we need to reliably identify the redundant and independent parameters. Thus, we need less noisy quantum hardware and low-overhead error mitigation techniques or even employ quantum error correction once the hardware is sufficiently advanced. On the other hand, DEA only optimizes parametric gates and thus needs to be combined with non-parametric gate optimization techniques. The latter usually use different principles than DEA which makes it difficult to combine the methods. Thus, a unified approach of DEA and non-parametric optimization techniques would be a major step forward.

Acknowledgments

Research at Perimeter Institute is supported in part by the Government of Canada through the Department of Innovation, Science and Industry Canada and by the Province of Ontario through the Ministry of Colleges and Universities. L.F. is partially supported by the U.S. Department of Energy, Office of Science, National Quantum Information Science Research Centers, Co-design Center for Quantum Advantage (C²QA) under contract number DE-SC0012704, by the DOE QuantISED Consortium under subcontract number 675352, by the National Science Foundation under Cooperative Agreement PHY-2019786 (The NSF AI Institute for Artificial Intelligence and Fundamental Interactions, <http://iaifi.org/>), and by the U.S. Department of Energy, Office of Science, Office of Nuclear Physics under grant contract numbers DE-SC0011090 and DE-SC0021006. S.K. acknowledges financial support from the Cyprus Research and Innovation Foundation under project “Future-proofing Scientific Applications for the Supercomputers of Tomorrow (FAST)”, contract no. COMPLEMENTARY/0916/0048. M.S. acknowledges the funding by the Helmholtz Einstein International Berlin Research School in Data Science (HEIBRiDS). P.S. acknowledges support from Agencia Estatal de Investigación (“Severo Ochoa” Center of Excellence CEX2019-000910-S, Plan National FIDEUA PID2019-106901GB-I00/10.13039 / 501100011033, FPI),, Fundació Privada Cellex, Fundació Mir-Puig, and from Generalitat de Catalunya (AGAUR Grant No. 2017 SGR 1341, CERCA program).

References

- [1] L. Funcke, T. Hartung, K. Jansen, S. Kühn and P. Stornati, *Dimensional expressivity analysis of parametric quantum circuits*, *Quantum* **5** (2021) 422.
- [2] L. Funcke, T. Hartung, K. Jansen, S. Kühn, M. Schneider and P. Stornati, *Best-approximation error for parametric quantum circuits*, *arXiv:2107.07378* (2021) [2107.07378].
- [3] J. Preskill, *Quantum Computing in the NISQ era and beyond*, *Quantum* **2** (2018) 79.
- [4] J. Biamonte, P. Wittek, N. Pancotti, P. Rebentrost, N. Wiebe and S. Lloyd, *Quantum machine learning*, *Nature* **549** (2017) 195.
- [5] R. Orús, S. Mugel and E. Lizaso, *Quantum computing for finance: Overview and prospects*, *Reviews in Physics* **4** (2019) 100028.
- [6] A. Montanaro, *Quantum algorithms: an overview*, *npj Quantum Information* **2** (2016) 15023.
- [7] F.G.S.L. Brandao and K.M. Svore, *Quantum speed-ups for solving semidefinite programs*, in *2017 IEEE 58th Annual Symposium on Foundations of Computer Science (FOCS)*, pp. 415–426, 2017, DOI.
- [8] M. Troyer and U.-J. Wiese, *Computational complexity and fundamental limitations to fermionic quantum monte carlo simulations*, *Phys. Rev. Lett.* **94** (2005) 170201.
- [9] F. Arute et al., *Quantum supremacy using a programmable superconducting processor*, *Nature* **574** (2019) 505.
- [10] H.-S. Zhong and et al., *Quantum computational advantage using photons*, *Science* **370** (2020) 1460.
- [11] K. Temme, S. Bravyi and J.M. Gambetta, *Error mitigation for short-depth quantum circuits*, *Phys. Rev. Lett.* **119** (2017) 180509.
- [12] A. Kandala, A. Mezzacapo, K. Temme, M. Takita, M. Brink, J.M. Chow et al., *Hardware-efficient variational quantum eigensolver for small molecules and quantum magnets*, *Nature* **549** (2017) 242.
- [13] S. Endo, S.C. Benjamin and Y. Li, *Practical quantum error mitigation for near-future applications*, *Phys. Rev. X* **8** (2018) 031027.
- [14] K. Yeter-Aydeniz, R.C. Pooser and G. Siopsis, *Practical quantum computation of chemical and nuclear energy levels using quantum imaginary time evolution and lanczos algorithms*, *npj Quantum Information* **6** (2020) 63.
- [15] L. Funcke, T. Hartung, K. Jansen, S. Kühn, P. Stornati and X. Wang, *Measurement error mitigation in quantum computers through classical bit-flip correction*, *arXiv:2007.03663* (2020) [2007.03663v1].

- [16] A. Peruzzo, J. McClean, P. Shadbolt, M. Yung, X. Zhou, P.J. Love et al., *A variational eigenvalue solver on a photonic quantum processor*, *Nat. Commun.* **5** (2014) 1.
- [17] J.R. McClean, J. Romero, R. Babbush and A. Aspuru-Guzik, *The theory of variational hybrid quantum-classical algorithms*, *New J. Phys.* **18** (2016) 023023.
- [18] Y. Wang et al., *Quantum simulation of helium hydride cation in a solid-state spin register*, *ACS Nano* **9** (2015) 7769.
- [19] C. Hempel et al., *Quantum chemistry calculations on a trapped-ion quantum simulator*, *Phys. Rev. X* **8** (2018) 031022.
- [20] C. Kokail et al., *Self-verifying variational quantum simulation of the lattice schwinger model*, *Nature* **569** (2019) 355.
- [21] T. Hartung and K. Jansen, *Zeta-regularized vacuum expectation values*, *J. Math. Phys.* **60** (2019) 093504.
- [22] K. Jansen and T. Hartung, *Zeta-regularized vacuum expectation values from quantum computing simulations*, *PoS (LATTICE 2019) 363* (2020) 153.
- [23] D. Paulson, L. Dellantonio, J.F. Haase, A. Celi, A. Kan, A. Jena et al., *Towards simulating 2d effects in lattice gauge theories on a quantum computer*, *arXiv:2008.09252* (2020) [2008.09252].
- [24] J.F. Haase, L. Dellantonio, A. Celi, D. Paulson, A. Kan, K. Jansen et al., *A resource efficient approach for quantum and classical simulations of gauge theories in particle physics*, *Quantum* **5** (2021) 393.
- [25] L. Zhao, Z. Zhao, P. Rebentrost and J. Fitzsimons, *Compiling basic linear algebra subroutines for quantum computers*, *arXiv:1902.10394* (2019) [1902.10394].
- [26] L. Funcke, T. Hartung, K. Jansen, S. Kühn, M. Schneider, P. Stornati et al., *Towards Quantum Simulations in Particle Physics and Beyond on Noisy Intermediate-Scale Quantum Devices*, *arXiv:2110.03809* (2021) [2110.03809].
- [27] G. Voronoi, *Nouvelles applications des paramètres continus à la théorie des formes quadratiques. premier mémoire. sur quelques propriétés des formes quadratiques positives parfaites*, *J. Reine Angew. Math* **133** (1908) 97.
- [28] G. Voronoi, *Nouvelles applications des paramètres continus à la théorie des formes quadratiques. deuxième mémoire. recherches sur les paralléloèdres primitifs*, *J. Reine Angew. Math* **134** (1908) 198.